The influence of micro-scale surface roughness on water-droplet contact electrification

L.E. Helseth

Department of Physics and Technology, Allegaten 55, 5020 Bergen, University of Bergen, Norway

ABSTRACT: When water comes in contact with a hydrophobic fluoropolymer, triboelectric charge tends to form on the surface. Here, it is investigated how the triboelectric charge formed upon contact with water drops depends on the micro-scale surface statistics of the polymer. In particular, it is found that the transition to a superhydrophobic fakir state results in a considerable reduction in triboelectric contact charge, due to a reduced liquid-solid contact area. Thus, when processing charge-sensitive electronic systems one may want to utilize such surfaces promoting reduced tribocharging. This also has implications for energy harvesting purposes, where one may collect electrical energy by letting water droplets move on the polymer with an interdigitated current-collecting electrode on its back side. In such a situation, it is observed that the surfaces promoting the superhydrophobic fakir state give rise to larger water droplet velocities and smaller collected charge, which explains the need for careful assessment of surface treatment before applying microstructured polymers for water droplet energy harvesting.

KEYWORDS: Fluoropolymer, wetting, triboelectric charge

1. Introduction

Contact electrification has been known for two thousand years, and is still an important research topic also today since many of the underlying mechanisms need to be better understood [1,2]. One particular issue of interest is how the microstructure changes the triboelectric charging of fluoropolymers [3].

Triboelectric charges formed on hydrophobic surfaces due to water in droplet form or due to laminar flow have been investigated for many decades [4-8]. While it appears that no universally accepted model explaining charge dynamics and magnitude have been found, there is evidence suggesting that preferential adsorption and/or orientation of O-H groups near the hydrophobic polymer surface play an important role [9-13]. Recent research has demonstrated that triboelectric charges induced by water can be used to harvest electrical energy for powering small electronic devices [14-27]. In such devices, one would often like to optimize the induced electrical charge in order to generate as much power as possible, while at the same time maximize the contact angle such that liquid droplets easily roll off and do not stick to the device. To achieve this, the surface roughness of many such surfaces has been altered in order to enhance the triboelectric charge or improve the wetting [14,17,21,23,27]. While some results suggest that low roughness and large contact area play a role [14,27], it is not clear how statistical parameters of the surface or the contact angle hysteresis influences the triboelectric charging. Indeed, the lack of systematic studies between wetting properties and triboelectric charge makes it hard to conclude which factors play the most important role when optimizing the charge and minimizing droplet stickiness. Here, a systematic study of randomly roughened surfaces of a fluoropolymer is undertaken to attempt to reveal such a correlation.

Surfaces with very large contact angles can be created in a variety of manners [28], in many cases inspired by Nature itself [29]. For example, one may create a rough surface by abrading fluorinated hydrophobic materials [30-33] or use particulates to create rough surfaces in curable liquid polymers such as polydimethylsiloxane [34-36]. In the current study, abrasion is chosen since it can be applied with very simple means to existing surfaces to get reasonably repeatable results when it comes to

surface statistics and wetting. This further allowed a study of the triboelectric charge that formed when water droplets moved over the rough surface with different types of electrodes.

2. Methods and experimental setup

Surface preparation: Fluorinated ethylene propylene (FEP) of thickness 127 μm, made by Dupont, was purchased from RS. The material was cut to sizes of typically 80 x 100 mm, and polished by hand using silicon carbide abrasive paper of grit size P60, P120, P180, P240, P320, P400, P800 and P1200. The applied force was of the order of 50 N, and the surface was polished until the polished pattern appeared homogenous and isotropic for the eye. The samples were rinsed carefully with water, then methanol, and then with water before use. The samples were also inspected visually and by microscope to ensure that no silicon carbide particles were present on the surface.

The mean roughness of the polished samples was obtained by taking pictures of the surfaces in a polarization microscope (Olympus BX60) with a resolution of about 0.5 μm. Microscope images from above as well as cross-sectional images were recorded. Figure 1 a) shows examples of two cross-sectional profile images of a film sanded with P180 (upper image) and a pristine FEP surface (lower image). In Fig. 1 b), the distribution of heights of the P180 surface is shown. While the root mean square deviations are about 23 μm for P180, they reduce to less than 2 μm for P1200. Thus, the latter surface is considerably smoother, but it is also seen from Fig. 1 a) that the P180-treated surface has characteristic threads which gives rise to large variations in the slope of the profile curve.

If h(x) is the height variation along the x-direction defined by the profile direction, one defines the slope as $s_x=dh/dx$. In Fig. 1 c) and d) the variations in s_x are shown for a surface treated with P1200 and P180 grit, respectively. In a given direction s_x or s_z along the surface, there is a distribution of slopes. One may define the local slope as $s = \sqrt{s_x^2 + s_z^2}$. The root mean square values of the height and slope variations

are defined as $h_{rms}=\langle h^2 \rangle$ and $h'_{rms} = \sqrt{\langle s_x^2 \rangle + \langle s_z^2 \rangle}$, respectively. From the one-dimensional profiles similar to those in Fig. 1 a) one obtains $h'_{xrms} = \sqrt{\langle s_x^2 \rangle}$. Typically, two or three such profile images have been evaluated for each sample. The root-mean square values of the slopes for different samples can then be obtained by assuming that the samples are isotropic such that $\langle s_x^2 \rangle = \langle s_z^2 \rangle$, which is found to be a reasonable assumption to within experimental uncertainty for the current samples. For an isotropic surface it then follows that $h'_{rms} = \sqrt{2} h'_{xrms}$.

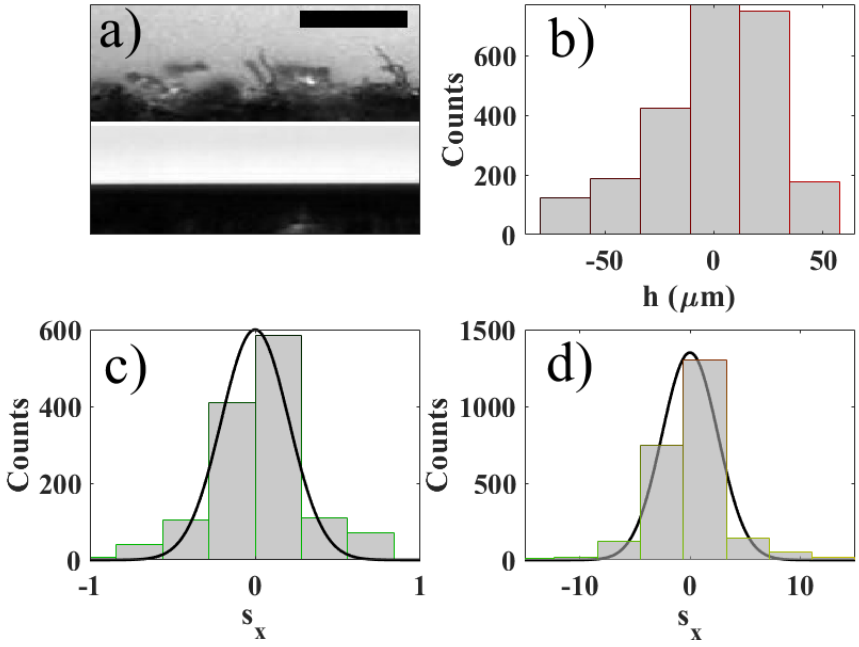

Figure 1. In a), example of profile images of FEP film sanded with P180 (upper part of image) or pristine (lower part of image) grit are displayed. The scale bar is 100 μm. In b) and d), the height and slope variations of the P180 sanded surface are shown, respectively. In c), the slope variations of P1200 sanded surfaces are shown. The black curves in c) and d) are gaussian fits to the data, with standard deviations of 0.3 and 3.6, respectively.

Contact angle measurements: Contact angle measurement were made using an OCA 20L contact angle measurement system using water droplets of volume 5 μL. This system can be used in either the tilted plate mode or injection-withdrawal method. The latter is based on injecting and withdrawing additional amounts of water from a small drop and observing the advancing and receding contact angles as the three-phase contact line starts to move. The tilted plate method allows one to record contact angles of a droplet deposited on a surface tilted which is no longer aligned perpendicular to the gravitational field, thus allowing one to obtain information about drop retention [37, 38]. It is known that the particular deposition method may influence the results of a tilted plate experiment, and the observed maximum and minimum observed contact angles do not necessarily represent the advancing and receding angles [38]. In the current study, surfaces with rather large water drop detention, which varied from place to place on the droplet, were observed. For many of the surfaces, the contact line did not move during injection of reasonable liquid volumes, as in the injection-withdrawal method, or tilting of the platform to 90°, as in the tilting plate method. It was therefore decided to record the difference $\Delta\theta = \theta_f - \theta_r$ between the maximum observed front contact angle θ_f (at the expected advancing contact line) and the minimum observed rear contact angle θ_r (at the expected receding contact line) during tilt of the platform. In addition, the static contact angle θ_s was also recorded.

Table I shows a summary of the abrasive paper used, the statistical parameters drawn from the surface as well as the wetting measurements. The author has not been able to find any studies of wetting on rough FEP made by abrasive sanding in the literature, but it might be useful to compare with an existing report on abraded Teflon [30]. The smooth FEP surface in the current study is so smooth that one cannot observe variations on a microscale with an optical microscope, while the Teflon surface in Ref. [30] was reported to have some initial roughness. Nonetheless, the roughness observed here is to a reasonable degree consistent with that reported in Ref. [30] on sanded Teflon surfaces. That is, the data in table I is comparable to that of Ref. [30] for grit sizes P180 to P800, while the roughness for grit size P60 shows

considerable deviation for reasons unknown to this author. The contact angle observations observed in the current study are also mostly comparable with those reported in Ref. [30], with the grit sizes P120, P180, P240 and P320 being able to generate static contact angles larger than 150°. It should also be noted that surfaces treated with grit size P120 were found to exhibit both larger (>150°) and smaller (down to 127°) static contact angles, depending on the position on the surface. These variations could be attributed to the manual polishing done to prepare the surfaces. However, randomly rough surfaces also result in formation of some larger FEP-fibres which may trap and alter the contact angle of the water droplets, and these fibers may be present for any type of polishing technique used. It should be pointed out that also reactive ion etching of FEP-surfaces lead to large variations in contact angle and hysteresis [39], and it is therefore possible that these features are to be expected for any surface treatment producing a more or less random distribution of sizes and slopes.

Grit	h_{rms} (μm)	h'_{xrms}	θ_s (°)	θ_f (°)	θ_r(°)	$\Delta\theta$ (°)	q (nC)
0	<0.1	<0.2	113±2	128±5	100±1	28±5	1.56±0.29
P60	29.3±8.9	1.9±0.8	120±5	130±4	109±3	21±5	1.54±0.15
P120	17.7±8.2	2.4±0.8	140±12	148±9	110±22	38±14	0.16±0.05
P180	23.1±4.0	5.0±2.0	150±2	150±10	125±20	25±22	0.25±0.06
P240	21.0±4.0	3.7±1.0	154±3	165±7	115±13	50±15	0.23±0.06
P320	14.8±1.0	2.3±0.2	151±6	162±6	124±17	38±18	0.34±0.05
P400	4.4±1.0	0.6±0.5	137±6	148±15	112±2	36±15	1.26±0.04
P800	3.5±1.0	1.3±0.5	135±3	146±11	110±4	36±12	1.41±0.10
P1200	1.9±1.1	0.2±0.2	129±5	141±5	112±5	29±7	1.40±0.21

Table I: The rms roughness (h_{rms}) and slope (h'_{xrms}) along one axis for different grit sizes. Also shown are the contact angles θ_s, θ_f and θ_r, the maximum contact angle difference $\Delta\theta$, and the contact charge q, for 5 μL water droplets.

Electrical characterization: The two setups used to determine triboelectric charge are shown in Figs. 2 a) and b). Deionized water of original resistivity 18.2 MΩcm was poured into a plastic container that fed a water dropper. The water was allowed to rest for a while in air, and the resistivity had by then dropped to roughly 1 MΩcm. The droplet rate was controlled manually by a valve, and was kept almost constant for all experiments. Small variations in the droplet rate were found not to influence any of the measurements.

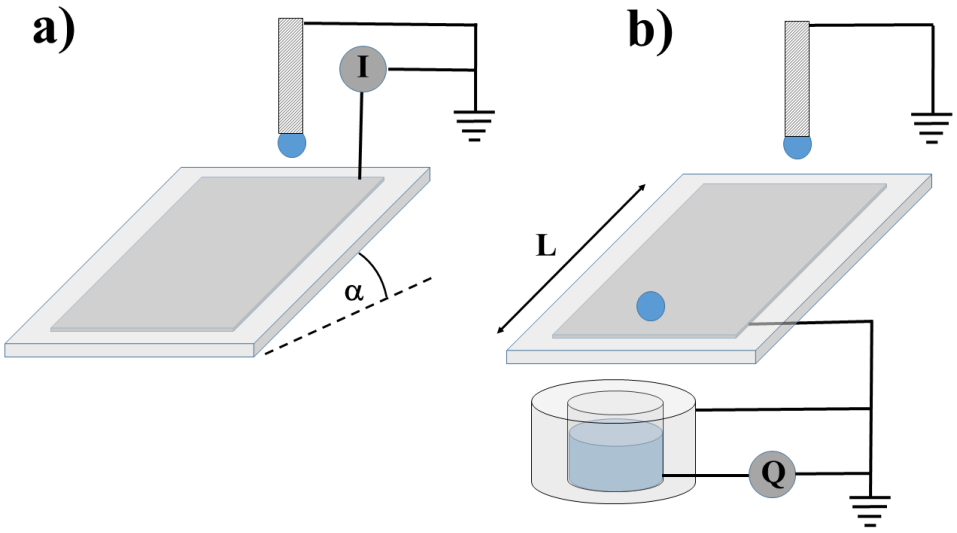

Figure 2. Setup for monitoring induced current in the electrode (a) and induced charge in the water drop (b).

The setup in Fig. 2 a) measures the induced current due to tribocharging, and utilizes an electrically earthed, metallized needle to drop water on a rough FEP surface. The FEP surface was angled at α=37° with the horizontal. This angle was selected since some of the surfaces had to be tilted at least 30° for the water drop to start moving. On the other hand, a larger surface tilt angle resulted in more unstable (wobbly) motion for some of the water drops which made it harder to obtain repeatable current pulses. The fall-

height of the drop is nearly zero, to remove the possibility of uncontrolled impact-induced tribocharges, see e.g. Refs. [40,41]. Directly under the FEP surface one places a metal surface in connection with an amperemeter (Keithley 6514 instrument). The current is measured for each drop of volume about 50 μL moving across the FEP surface and passing over the electrode edges. As detailed in Ref. [41], the current pulse occurs when the water droplet passes over the electrode edge. The charge associated with the induced current in the electrode is found using $q = \int Idt$.

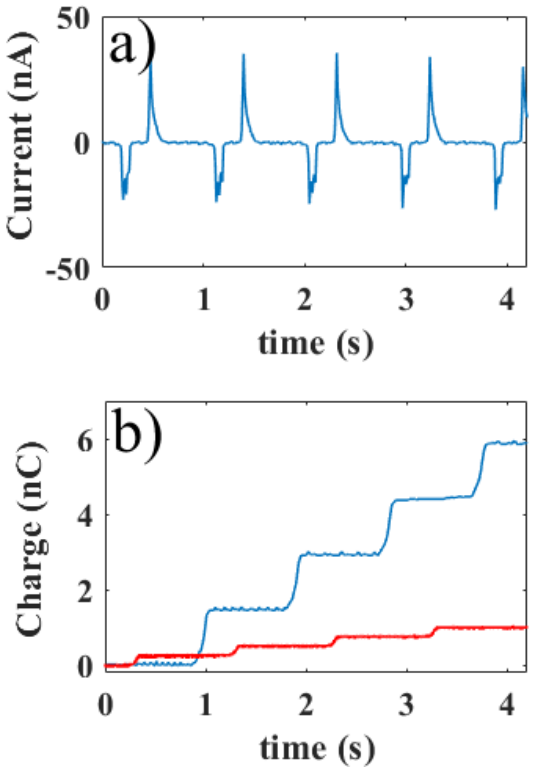

Figure 3. In a), the current of a pristine FEP surface measured using the setup in Fig. 2 a) is shown. In b), the charge for a pristine (blue line) and P180-abraded (red line) surface measured using the setup in Fig. 2 b) is shown.

The induced charge in the water drop after moving over the FEP surface was measured using the setup in Fig. 2 b). Here, the metal surface under the FEP surface is earthed and connected to the outer metal cup

of a Faraday cage as shown. The water droplets fall into the inner metal cup, which is connected to an electrometer (Keithley 6514 instrument) measuring the induced charge in each drop. Figure 3 a) shows the current of a pristine FEP surface measured using the setup in Fig. 2 a). When the droplet comes in contact with the FEP surface, a positive charge occurs in the water still in contact with the metallized needle, and a current will flow. When the water droplet moves over the edge of electrode, a current of opposite sign occurs since the positive charge of the droplet that was a part of the electric double layer is now replaced by positive charge in the metal. A more detailed explanation is given in Refs. [6,7,40,41]. The first contact between the FEP surface and the drop is not a clean, single touch, but may exhibit fluctuations which give rise to more than a single current peak. The exit of the droplet from the electrode edge does on the other hand not exhibit such fluctuations, thus leading to a sharp, single peak. Note that the positive and negative current pulses cover the same area under the curve in Fig. 3 a), such that charge is conserved. To find the charge induced in the electrode after the droplet has moved over the FEP surface, one may integrate the positive current pulse with time.

Fig. 3 b) shows the charge measured using the setup in Fig. 2 b) for a pristine (blue line) and P180-abrade (red line) FEP surface. Each step represents a droplet, and it is seen that while the pristine FEP surface gives rise to droplets exhibiting net charge about +1.5 nC, the water droplets moving over the surface abraded with grit P180 exhibit a charge of only +0.3 nC. The temperature was about 20 °C during the measurements. The measurements of charge using the setup in Fig. 2 b) are given in table I. The measurements were undertaken on three different samples for some grit sizes (pristine FEP, P180 and P1200), and two samples for other grit sizes. In all cases, the measurements were repeated multiple times (at least three) on each sample. Figure 4 plots the charge obtained the setup in Fig. 2 a) (red circles) and the setup in Fig. 2 b) (black squares) as a function of static contact angle θ_s.

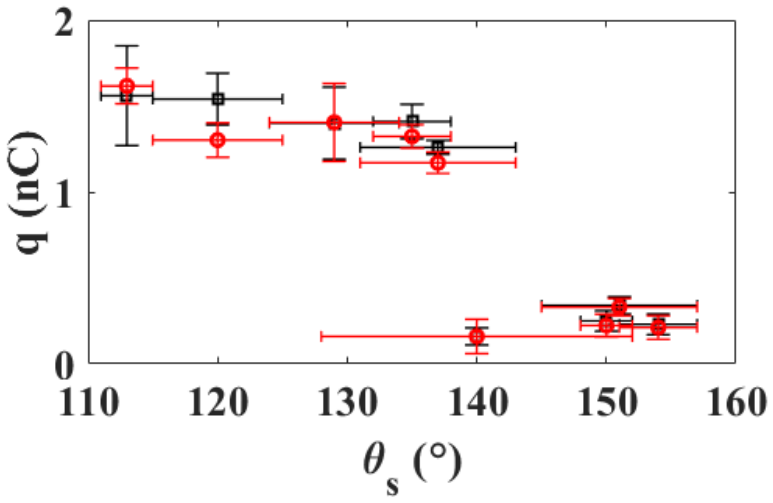

Figure 4. The charge gathered from a Faraday cup (black squares) and current measurements (red circles) as a function static contact angle.

3. Triboelectric charges

The transition from a fully wetting Wenzel-state [42] to a Cassie-Baxter state fakir state where there is air between the water droplet and the fluoropolymer [43], occurs when the roughness becomes larger than a critical value [44-48]. In ref. [46] it was found that a robust criterion for superhydrophobicity is when the roughness is larger than -1/cosθ_Y, where θ_Y is the static contact angle on a smooth surface, which gives the following approximate requirement; $h'_{xrms} > \sqrt{\pi/(2cos^2\theta_Y)}$. Inserting θ_Y=113° from table I, this requirement becomes h'_{xrms}>3.2. According to table I, only the surfaces abraded by P180 and P240 grit fulfill this condition, and it is indeed found experimentally that only these two surfaces have contact angles larger than 150° with a rolloff angle that in some places on the surface could be smaller than 5°. While the contact angle remains large for all parts of the surface, there was considerable variations in drop retention, possibly due to the single hair-like structures in Fig. 1 a) possibly also acting as trapping sites. Also notable is that while the surfaces treated with grit size P120 and P320 have large surface slope variations approaching 3.2, they do not fulfill this condition despite exhibiting contact angles larger than 150°. It is possible that details in the surface and small deviations from ideal gaussian statistics play a role

in this deviation, and that more elaborate theories outside the scope of the current study would be able to account for superhydrophobicity at lower slope variations as well.

Despite the increased gravitational force, it was observed experimentally that for larger 50 µL drops only the surfaces sanded with P120, P180, P240 and P320 grit exhibited static contact angles larger than 150°, as was also observed for 5 µL drops. The 5 µL drops produced a rather small electrical signal, with a small signal to noise ratio, which made larger 50 µL drops the appropriate choice when doing measurements of charge.

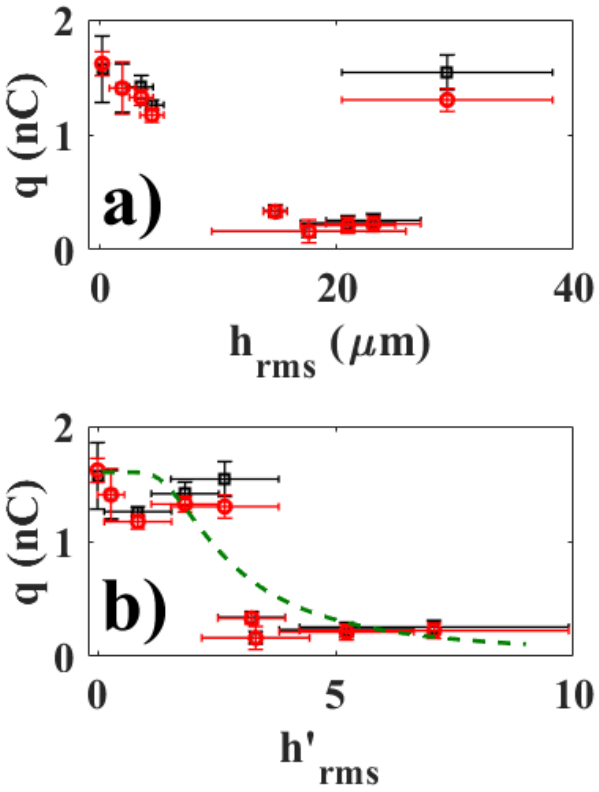

Figure 5. The charge gathered from a Faraday cup (black squares) and current measurements (red circles) as a function of rms roughness (a) and slope (b). The dashed green line is a fit to Eq. (2) with θ_Y=113° and q_0=1.6 nC.

The charge was measured using the setups in Fig. 2 a) and b) from about ten pulses or steps, each corresponding to a droplet, repeated four times at different days under similar environmental conditions. Figure 5 a) shows the charge measured using the current measurements (red circles) in Fig. 2 a) and the Faraday cup (black squares) in Fig. 2 b) as a function of surface roughness. Two observations can be made from Fig. 5 a). First, it is seen that the charge measured using the Faraday cup and the current measurement system are in agreement to within the uncertainty of the measurements. This validates that the charge induced in the metal electrode in all cases is equal to the net charge transferred to the droplet. Second, it is seen that the charge does not scale with roughness. That is, the two samples abraded with P180 and P240 grit exhibiting medium roughness and the largest contact angles give rise to the smallest triboelectric charge. Instead, the charge appears to be decreasing with root-mean-square of the slope in a nonlinear manner as observed in fig. 5 b), and the transition from large to small tribocharge occurs for a slope around 4. Increasing the slope gives rise to a fakir state with strongly reduced liquid-solid contact area, which gives rise to reduced charge and large contact angles. At this point, one may also note from Fig. 4 that there is a relationship between charge and contact angle. However, since the latter is determined by the the surface statistics, it makes sense to attempt to relate the tribocharge to the surface statistics in a direct manner.

The changes in electrical charge with wetting properties as seen in Fig. 5 can to some degree be explained by considering wetting theory on statistically random surfaces [46,47]. If A_0 is the apparent liquid-solid contact area for a pristine surface and A_1 is the projected contact area for a rough surface, the effective liquid-solid area fraction is given by $\phi = A_1/A_0$. We assume further that the transferred charge is proportional to the area fraction ϕ, i.e. $q \propto \phi$. From the experimental data it is hypothesized that the micron-scale height variations play a less significant role in forming the triboelectric charge. One may expect an increase in the contact area if a fully wetted Wenzel state could be maintained. However, for the micron to millimeter scale surface roughnesses studied here it appears that such an increase in roughness has negligible influence on the induced charge, as observed in Fig. 5 a). Instead, the distribution

of slopes plays a significant role since these are responsible for the formation of the fakir state with reduced contact area.

In a given direction s_x or s_z along the surface, the distribution of slopes is assumed to be random (gaussian). From. Fig. 2 c) and d), it is seen that this is a reasonable assumption, although some deviations from a gaussian is seen. If the surface is isotropic, one may define the local slope as $s = \sqrt{s_x^2 + s_z^2}$. The local slope must fulfill $s<s_Y=-\tan\theta_Y$ [44], and the statistics is assumed to be governed by a Rayleigh distribution [45-47]

$$p(s) = \frac{2s}{h_{rms}^2} exp\left(-\frac{s^2}{2h_{rms}'^2}\right) \quad . \tag{1}$$

Neglecting roughness variations, the surface area can be approximated by $\phi \approx \frac{1}{2}\int_0^{s_Y} p(s)ds$, where the factor 1/2 is included to disregard regions with positive curvature. In the current work it is assumed that the charge scales with the contact area, $q \propto \phi$, such that the triboelectric charge can be found as

$$q \approx q_0 \left[1 - exp\left(-\frac{tan^2\theta_Y}{h_{rms}'^2}\right)\right] \quad , \tag{2}$$

where q_0 is the charge of a pristine surface. In Fig. 5 b), the green dashed line is a fit to the experimental data with θ_Y=113° (from table I) and q_0=1.6 nC. The transition from a hydrophobic wetting state to superhydrophobic fakir state occurs in the range of h'_{rms} around 4 while application of Eq. (2) suggests that the transition should occur more gradually and start at slightly smaller values of the root-mean-square-slope. In particular, it is seen that there is an overlap in the estimated values of the slope for samples treated with grit size P60 and P320, while the contact charges measured for these two samples are very different. On the other hand, samples treated with grit size P60 never exhibited contact angles above 150°

as those treated with P320 did. Due to the presence of outlying fibers acting as trapping sites, considerable variations in surface slopes and contact angles occur for samples treated in the manner done here. On the other hand, the surface does either give rise to a Cassie-Baxter state or a Wenzel state. Since Eq. (2) is an idealization for a perfectly randomly rough surface that does not account such variations, it does not allow one to describe the sharp transition seen in Fig. 5 b). Thus, Eq. (2) aids a qualitative, but perhaps not a quantitative understanding of how the roughness governs the triboelectric charge. It should also be emphasized that Eq. (2) is only a reasonable approximation as long as the surface roughness does not contribute significantly to an increased charge and as long as the charge density remains constant and independent of the particular geometry encountered. The current experimental work appears to support such an interpretation, but it is possible that other systems were roughness or chemical composition varies on the nanoscale may behave differently.

4. Charge induced in interdigitated electrodes

It has been found advantageous to use interdigitated electrodes when harvesting electrical energy from water droplets, since each electrode finger pair allows collection of charge corresponding to that of the single electrode [40,41]. An interesting question is how surface roughness changes the current and charge recorded by interdigitated electrodes. Figure 6 shows the experimental setup used here. It resembles that of Fig. 2 a), but now an interdigitated electrode of 4 pair of fingers is used as the electrode instead of a plane metal surface. The interdigitated electrode was made in aluminum by UV-lithography such that each electrode finger was 4 mm wide and had a gap of 4 mm between them. The length of the fingers was much larger than the width. The metallized water dripper was connected to earth, as was also the first finger electrode the droplet moved over.

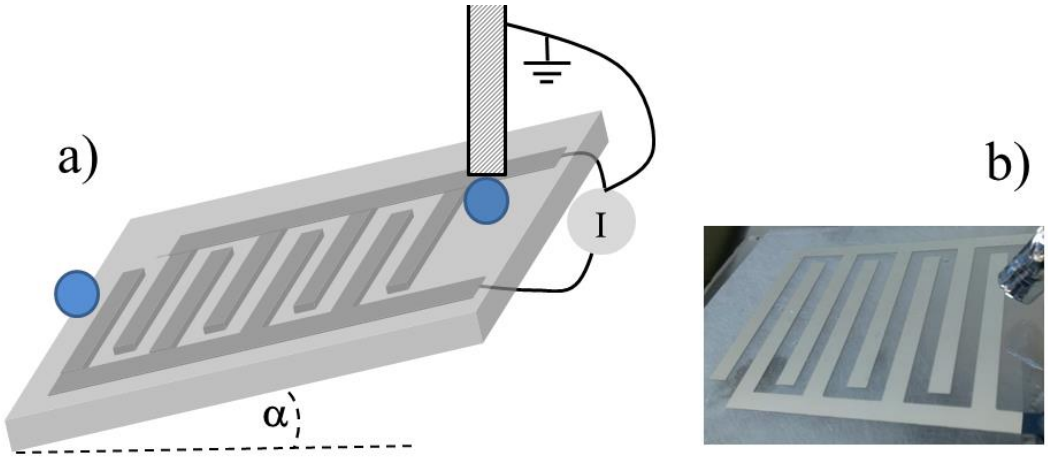

Figure 6. Schematic drawing of setup for monitoring current and induced charge on interdigitated electrodes (a), as well as a picture of the dropper and the IDE electrode mounted on the back side of an FEP surface abraded with P180 grit (b). The metal-covered dropper was earthed and connected to the first electrode of the interdigitated electrode.

Figure 7 a) shows the current induced in the interdigitated electrodes for pristine (solid line) and P180 grit-treated (dashed line) FEP surfaces. It is seen that the current peaks reach about 80 nA for the pristine surface, while the superhydrophobic surface treated with P180 grit it is only about 50 nA. In Fig. 7 b), the velocity of the 50 μL droplets was obtained by measuring the time it took to move from the third to the forth finger of the electrode. This fixed position was selected since this gave the highest measurable velocity for droplets using this method, but also other fingers could have been selected which gave similar results. As expected, the droplets on the rough surfaces with the highest contact angles gave rise to the largest velocities. The large velocity is caused by the reduced friction experienced by the droplet in the fakir state, moving partially on an air-cushion down the incline.

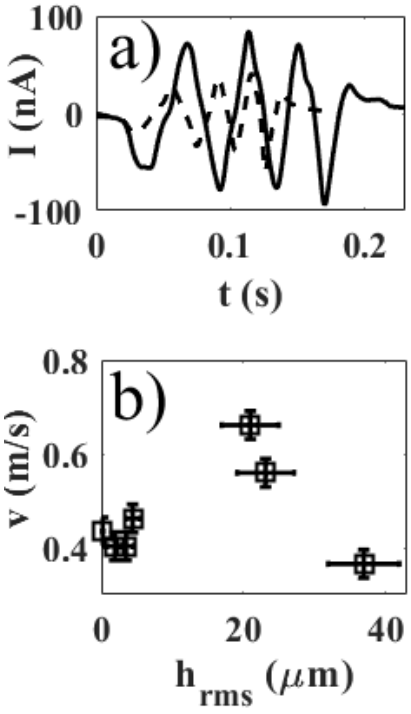

Figure 7. The current generated by a 50 μL droplet moving over the interdigitated electrodes of a pristine (solid line) and P240 sanded (dashed line) FEP surface (a). The velocity of the droplet moving between 3rd and 4th finger of the electrode as a function of surface roughness (b).

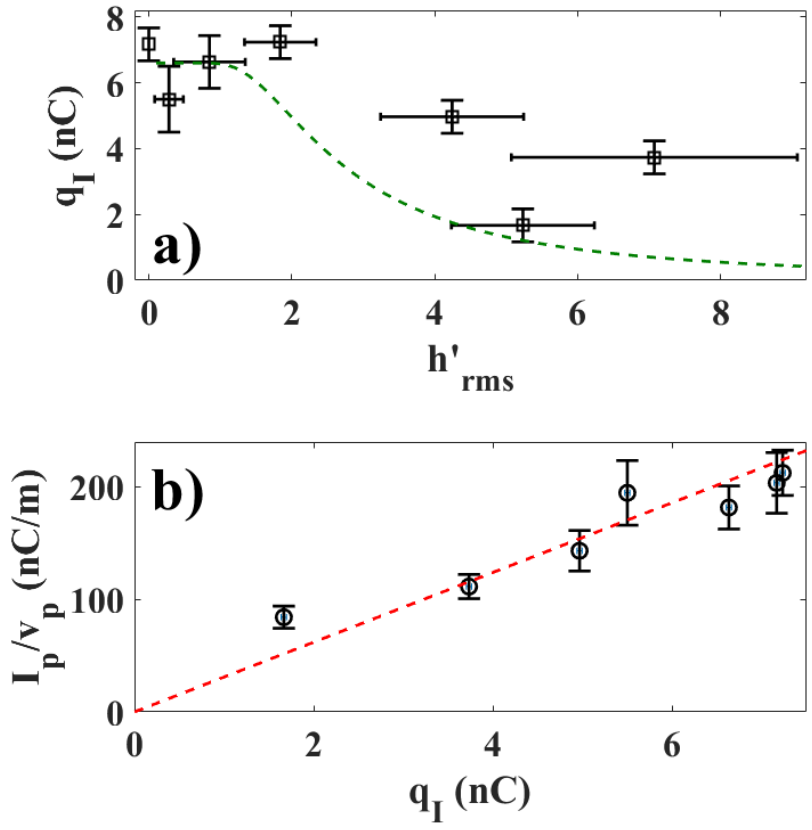

Figure 8. The charge gathered from current measurements using and interdigitated electrode (a). The dashed green line is a fit to Eq. (2) with θ_Y=113° and q_0=6.6 nC. In b), the peak current divided by velocity is shown as a function of measured charge. The dashed red line is a linear fit to the experimental data.

Using the data for current (I) versus time, the total induced charge (q_I) in the interdigitated electrodes could be found using $q_I = \int |I| dt$. Here, the absolute sign (|I|) is taken since the induced current changes sign as the water drop moves of alternating electrode fingers. Integrating without the absolute sign would result in zero charge, while including it allows one to compare the charge induced of a single electrode as shown in Fig. 5. The data in Fig. 8 a) shows the induced charge as function of the measured root mean square slope. The green, dashed line is a fit of Eq. (2) to the experimental data with θ_Y=113° and q_0=6.6 nC. The transition from large to small charge is not as noticeable as in Fig. 5 b), but it appears to occur at

a root-mean-square slope between 4 and 5. In the case of a single electrode in Fig. 5 b), the induced charge of pristine FEP was 1.6 nC, which is 6.6/1.6≈4 times smaller than that observed in Fig. 8 a). The total charge induced, which also represents the charge the particular geometrical arrangement of the interdigitated electrodes selected here can collect, should just be four times that of a single electrode, since there are four fingers corresponding to single electrodes. A significant deviation from Eq. (2) and the data for a single electrode in Fig. 5 b) is that the charge induced in an FEP surface treated with grit size P180 and P240 and collected by interdigital electrodes is significantly larger (3.8 nC and 2.0 nC, respectively) than that expected from Fig. 4 b) (4 x 0.25 nC = 1.0 nC and 4 x 0.23 nC = 0.92 nC, respectively). While the exact reason for this deviation is not known, it is possible that the induced charge gathered by the interdigital electrodes are more sensitive to the velocity as the droplets pass by, such that an increased velocity means larger induced charge. In the single electrode measurement mode of Fig. 5 b), such a velocity-induced charge plays a smaller role, since the charge is accumulated while the droplet moves over the FEP surface, and is not influenced by the uniform electrode. According to Fig. 7 b), FEP surfaces treated with grit size P180 and P240 have roughly 1.5-1.7 times larger velocity than pristine surfaces. If there was a linear dependence between induced charge and velocity, this could explain much of the increased charge seen for the surface treated with grit size P240. However, for the surface treated with grit size P180, a linear relationship between velocity and induced charge could not explain the observations. The details are probably hidden in the interaction between the fluctuating and moving droplet as it interacts with the electrodes on its way down, but further computational studies outside the scope of this work are needed to reveal such details.

The peak current in Fig. 7 a) is the largest observed current for each FEP surface. In Fig. 8 b), the peak current I_p divided by the measured velocity is plotted as a function of the induced charge q_I. It is observed that there is a nearly linear trend, which can be explained by noting that the current is given by $I=dq/dt$, where $q=\sigma A$, σ is the surface charge density and A is the area. The area can be approximated by $A\approx Lx$, where L is the width of the droplet and x is displacement of it over the electrode finger. Thus, we find the

current to be $Ip=\sigma L dx/dt$, where $v=dx/dt$ is the droplet velocity. The peak current divided by the peak velocity $v=v_p$ is therefore proportional to the surface charge density σ, which again is proportional to the total induced charge q_I for a given surface, i.e. $I_p \propto q_I$. The dashed line in Fig. 8 b) shows a linear fit to the experimental data with $I_p/v=aq_I$ and $a=31\ m^{-1}$. Although some deviation of experimental data from the linear trend is observed, the overall impression that surface charge density is nearly constant is strengthened.

Minimizing contact charging is a crucial issue for electronics, friction and wear, and several novel methods have recently been developed to avoid these using solid materials [49,50]. In most situations, only very nonconductive liquids exhibit significant contact electrification. However, if fluoropolymers coming in contact with deionized water drops are used to process sensitive electronics, one may also be interested in minimizing the triboelectric charge [6,7]. As shown in the current study, roughening of the surface with a sufficiently large variation of slopes may provide a simple and cost-effective method for reducing the tribocharge and at the same time removing water more efficiently. One may also imaging that gradients of wettability as obtained by spatially located sanded patterns would allow one to control the charge and velocity of droplets, thus adding to the continuously growing toolbox for controlling and functionalizing droplets [51].

5. Conclusion

In this study, it has been demonstrated that the micron scale roughness of a fluoropolymer surface has significant influence on its ability to transfer charge due to water droplets moving across it. The measurements indicate that large variations in surface slope are needed to create large static contact angles, and that this also results in comparably small triboelectric charge for water droplets moving over the surface. Such micro-structured surfaces may be generated in cost-effective manner using manual or

machine-guided sanding, and could be advantageous in situations where one would need to minimize the triboelectric charge when water is flowing across the fluoropolymer. Pristine or finely abraded surfaces gave the largest triboelectric charge, and would therefore be of most interest for energy harvesting purposes. It should also be pointed out that the current study has only considered microtextured surfaces, and it might be that the situation changes if one has a fully wetting Wenzel state combined with considerably enhanced surface area due to nanotexturing. Future work may involve further studies on nanoscale surface textures, possibly containing charged surface groups exhibiting slope or roughness gradients, in order to obtain further insight into the formation of triboelectric charges.

REFERENCES

(1) D.J. Lacks and R.M. Sankaran, "Contact Electrification of Insulating Materials" J. Phys.D. Appl. Phys. **2011**, 44, 453001.

(2) S. Pan and Z. Zhang, "Fundamental theories and basic principles of triboelectric effect: A review", Friction, **2019,** 7, 2-17.

(3) A.E. Wang, P.S. Gil, M. Holonga, Z. Yavuz, H.T. Baytekin, R. Mohan Sankaran and D.J. Lacks, Dependence of triboelectric charging behaviour on material microstructure", Phys. Rev. Mat., **2017**, 1 035605.

(4) I. Langmuir, "Surface electrification due to recession of aqueous solutions from hydrophobic surfaces", J. Am. Chem. Soc., **1938**, 60, 1190-1194

(5) R. Williams, "The relation between contact charge transfer and chemical donor properties", J. Coll. Int. Sci., **1982**, 88, 530-535.

(6) M. Matsui, N. Murasaki, K. Fujibayashi, P.Y. Bao and Y. Kishimoto, “Electrification of pure water flowing down a through set up with a resin sheet”, J. Electrostatics, **1993**, 31, 1-10.

(7) K. Yatsuzuka, Y. Mizuno and K. Asano, “Electrification phenomena of pure water droplets dripping and sliding on a polymer surface”, J. Electrostatics, **1994**, 32, 157-171.

(8) T.A.L. Burgo, F. Galembeck and G.H. Pollack, “Where is water in the triboelectric series”, J. Electrostatics, **2016**, 80, 30-33.

(9) M. Chaplin, Water, ”Theory vs. experiment: What is the surface charge of water”, **2009**, 1, 1-28.

(10) J.K. Beattie, “The intrinsic charge on hydrophobic microfluidic substrates”, Lab Chip, **2006**, 6, 1409-1411.

(11) K.N. Kudin, R. Car, “Why are water-hydrophobic interfaces charged”, J. Am. Chem. Soc., **2007**, 130, 3915-3919.

(12) V. Tandon, S.K. Bhagavatula, W.C. Nelson and B.J. Kirby, “Zeta potential and electroosmotic mobility in microfluidic devices fabricated from hydrophobic polymers:1. The origin of charge”, Electrophoresis, **2008**, 29, 1092-1101.

(13) S. Strazdaite, J. Versluis and H.J. Bakker, “Water orientation at hydrophobic interfaces”, J. Chem. Phys., **2015**, 143, 084708.

(14) Z.H. Lin, G. Cheng, L. Lin, S. Lee and Z.L. Wang, “Water-solid surface contact electrification and its use for harvesting liquid wave energy”, Angew. Chem. Int. Ed. **2013**, 52, 1-6.

(15) J. K. Moon, J. Jeong, D. Lee, and H. K. Pak, “Electrical power generation by mechanically modulating electrical double layers” Nat. Commun. **2013**, 4, 1487.

(16) S.-H. Kwon; J. Park, W.K. Kim, Y. Yang, E. Lee, C.J. Han, S.Y. Park, J. Lee and Y.S. Kim, "An effective energy harvesting method from a natural water motion active transducer", Energy Environ. Sci., **2014**, 7, 3279-3283.

(17) Z.H. Lin, G. Cheng, S. Lee, K.C. Pradel and Z.L. Wang, "Harvesting water drop energy by sequential contact electrification and electrostatic induction process", Adv. Mater **2014**, 26, 4690-4696.

(18) L. Zheng, Z.H. Lin, G. Cheng, W. Wu, X. Wen, S. Lee and Z.L. Wang, "Silicon-based hybrid cell for harvesting solar energy and raindrop electrostatic energy", Nano Energy, **2014**, 9, 291-300.

(19) Q. Liang, X. Yan, Y.Gu, K. Zhang, M. Liang, S. Liang, X. Zheng and Y. Zhang, "Highly transparent triboelectric nanogenerator for harvesting water-related energy reinforced by antireflection coating", Scientific Reports, **2015**, 26, 4690-4696.

(20) S.B. Jeon, D. Kim, G.-W. Yoon, J.-B. Yoon and Y.-K. Choi, "Self-cleaning hybrid energy harvester to generate power from raindrop and sunlight", Nano Energy, **2015**, 12, 636-645.

(21) G. Zhu, Y. Su, P. Bai, J. Chen, Q. Jing, W. Yang and Z.L. Wang, 'Harvesting water wave energy by asymmetric screening of electrostatic charges on a nanostructured hydrophobic thin-film surface', ACS Nano, **2014**, 8, 6031-6037.

(22) J. Han, B. Yu, G. Qu, H. Chen, Z. Su, M. Shi, B. Meng, X. Cheng and H. Zhang, "Electrification based devices with encapsulated liquid for energy harvesting, multifunctional sensing, and self-powered visualized detection", J. Mater. Chem. A, **2015**, 3, 7382-7388.

(23) D. Choi, S. Lee, S.M. Park, H. Cho, W. Hwang and D.S. Kim, "Energy harvesting model of moving water inside a tubular system and its application of a stick-type compact triboelectric nanogenerator", Nano Research, **2015**, 3, 7382-7388.

(24) J. Park, Y. Yang, S.-H. Kwon and Y.S. Kim, “Influences of surface and ionic properties on electricity generation of an active transducer driven by water motion”, J. Phys. Chem. Lett., **2015**, 6, 745-749.

(25) L.E. Helseth and X.D. Guo, “Contact electrification and energy harvesting using periodically contacted and squeezed water droplets”, Langmuir. **2015**, 31, 3269-3276.

(26) Y. Sun, X. Huang and S. Soh, “Using the gravitational energy of water to generate power by separation of charge at interfaces”, Chem. Sci., **2015**, 6, 3347-3353.

(27) J.W. Lee and W. Hwang, “Theoretical study of micro/nano roughness effect on water-solid triboelectrification with experimental approach”, Nano Energy, **2018**, 52, 315-322.

(28) J.T. Simpson, S.R. Hunter og T. Aytug, “Superhydrophic materials and coatings: a review”, Rep. Prog. Phys. **2015**, 78, 086501.

(29) W. Barthlott og C. Neinhus, “Purity of the sacred lotus, or escape from contamination in biological surfaces”, Planta, **1997**, 202, 1-8.

(30) M. A. Nilsson, R.J. Daniello and J.P. Rothstein, “A novel and inexpensive technique for creating superhydrophobic surfaces using Teflon and sandpaper”, J. Phys. D: Appl. Phys., **2010**, 43, 045301.

(31) D. Song, R.J. Daniello and J.P. Rothstein, “Drag reduction using superhydrophobic sanded Teflon surfaces”, Exp. Fluids, **2014**, 55, 1783.

(32) F. Wang, S. Yu, J. Ou, M. Xue and W. Li, “Mechanically durable superhydrophobic surfaces prepared by abrading”, J. Appl. Phys., **2013**, 114, 124902.

(33) F.J. Wang, C.Q. Li, Z.S. Tan, W. Li, J.F. Ou and M.S. Xue, “PVDF with stable superhydrophobicity”, Surface&Coatings Technology, **2013**, 222, 55-61.

(34) Y.T. Lin and J.H. Chou, “A low-cost filler-dissolved process for fabricating super-hydrophobic poly(dimethylsiloxane) surfaces with either lotus or petal effect”, J. Micromech. Microeng., **2014**, 24, 055021.

(35) Y.T. Lin and J.H. Chou, “Fabricating translucent polydimethylsiloxane (PDMS) superhydrophobic surface greenly by facile water-dissolved fillers”, J. Adhesion Sci. Technol., **2016**, 30, 1310-1318.

(36) H. Tian, F. Wang, S. Ge, J. Ou, W. Li and S. Yu, “A simple and effective way to fabricate mechanical robust superhydrophobic surfaces”, RSC Advances, **2016**, 6, 28563.

(37) C.G.L Furmidge. “Studies at phase interfaces. I. The sliding of liquid drops on solid surfaces and a theory for spray retention”. Journal of Colloid Science, **1962**, 17.4, 309 –324.

(38) E. Pierce, F.J. Camora and A. Amirfazli, “Understanding of sliding and contact angle results in tilted plate experiments”, Colloids and Surfaces A, **2008**, 323, 73-82.

(39) N. Frøvik, M.M. Greve and L.E. Helseth, “Nanostructures and wetting properties controlled by reactive ion etching of fluorinated ethylene propylene”, Colloids and Surfaces A, **2019**, 574, 228-238.

(40) L.E. Helseth and X.D. Guo, “Hydrophobic polymer covered by a grating electrode for converting the mechanical energy of water droplets into electrical energy”, Smart Mat. Structures, **2016**, 25, 045007.

(41) L.E. Helseth, “Electrical energy harvesting from water droplets passing a hydrophobic polymer with a metal film on its back side”, J. Electrostat., **2016**, 81, 64-70.

(42) R.N. Wenzel, “Resistance of solid surfaces to wetting by water”, Ind. Eng. Chem., **1936**, 28, 988-994.

(43) A. Cassie and S. Baxter, "Wettability of porous surfaces", Trans. Faraday Soc., **1944**, 40, 546-551.

(44) C. Yang, U. Tartaglino and B.N. Persson, "Nanodroplets on rough hydrophilic and hydrophobic surfaces", Eur. Phys. J. E, **2008**, 25, 139-152.

(45) R. David and A.W. Neumann, "Contact angle hysteresis on randomly rough surfaces: A computational study", Langmuir, **2013**, 29, 4551-4558.

(46) F. Bottiglione and G. Carbone, "Role of statistical properties of randomly rough surfaces in controlling superhydrophobicity", Langmuir, **2013**, 29, 599-609.

(47) L. Afferante and G. Carbone, "Statistical theory of wetting of liquid drops on superhydrophobic randomly rough surfaces", Phys. Rev. E, **2015**, 92, 042407.

(48) L. Afferante and G. Carbone, "Effects of drop volume and surface statistics on the superhydrophobicity of randomly rough substrates", J. Phys.: Condens. Matter, **2018**, 30, 045001.

(49) H.T. Baytekin, B. Baytekin, T.M. Hermans, B. Kowalczyk and B.A. Grzybowski, "Contro, of surface charges by radicals as a principle of antistatic polymers protecting electronic circuitry", 2013, 341, 1368-1371.

(50) K. Sayfidinov, S. D. Cezan, B. Baytekin and H.T. Baytekin, "Minimizing friction, wear, and energy losses by eliminating contact charging", Sci. Adv., **2018**, 4, eaau3808

(51) S. Lach, S.M. Yoon and B.A. Grzybowski, "Tactic, reactive, and functional droplets outside of equilibrium", Chem. Soc. Rev., **2016**, 45, 4766.